



Direct regeneration of NADH on a ruthenium modified glassy carbon electrode

Amir Azem, Felise Man, Sasha Omanovic*

Department of Chemical Engineering, McGill University, 3610 University St., Montreal, Que., Canada H3A 2B2

Received 4 March 2004; received in revised form 27 April 2004; accepted 27 April 2004

Abstract

The regeneration of NADH in a batch electrochemical reactor using a ruthenium modified glassy carbon electrode (RuGC) has been investigated. The information on the structure of the electrode/electrolyte interface in the presence of NAD^+ in the solution, the kinetics of NAD^+ reduction, and the batch-electrolysis NADH regeneration has been obtained using electrochemical techniques of dc linear potential (LP) and constant potential (CA) polarization, ac differential capacitance (DC), and electrochemical impedance spectroscopy (EIS). It has been shown that the modification of GC by a sub-monolayer of Ru can provide an electrode surface capable of reducing NAD^+ directly to NADH at a high yield of enzymatically active 1,4-NADH (96%). From the electrochemical point of view, the reaction is irreversible and occurs at high cathodic overpotentials, where the reaction rate is controlled by the surface diffusion of electroactive species. EIS measurements have shown that the electrode/electrolyte interface and the corresponding charge- and mass-transfer processes can be described by an electrical equivalent circuit composed of two time constants in parallel, with the additional contribution of a mass-transport Warburg impedance element. The time constant recorded at higher frequencies represents the response of a GC part of the electrode surface, while the lower-frequency time constant can be related to the response of Ru sites on the electrode surface. It has been determined that the NAD^+ reduction reaction is of first order with respect to NAD^+ . The calculated apparent heterogeneous reaction rate constant values are rather low, which is due to the slow mass-transport of electroactive species at the electrode surface. The kinetic analysis has demonstrated that a very good agreement between the apparent heterogeneous reaction rate constant values calculated using three different experimental techniques is obtained.

© 2004 Elsevier B.V. All rights reserved.

Keywords: NADH regeneration; NAD^+ electroreduction; Ruthenium modified glassy carbon; Kinetics; Electrochemical techniques

1. Introduction

In a large number of biotechnological enzyme-catalyzed processes, with the exception of the use of a base enzyme, a corresponding coenzyme (cofactor) has to also be used. Nicotinamide adenine dinucleotide NAD(H) (Scheme 1) is a cofactor that is involved in a large number of biochemical processes. It acts as an electron and hydrogen donor in most of the biochemical reactions catalyzed by redox enzymes (dehydrogenases or oxidoreductases). In its reduced and enzymatically active form (1,4-NADH), the molecule transfers two electrons and a proton to a substrate in the presence of a suitable enzyme to form NAD^+ . The high cost

of NADH requires that the molecule be regenerated in situ when used in a bioreactor, and this has been the major motivation for research in the development of in situ NADH regeneration techniques. The major regeneration approaches that have been used so far are outlined in the following text.

In their review paper on regeneration of NADH for use in organic synthesis, Chenault and Whitesides [1] summarized a number of different techniques employed to regenerate NADH. The paper discusses factors influencing the stability and lifetime of NADH in a solution, as well as process considerations that are relevant to the use of NADH in synthesis. The authors have shown that electrochemistry offers a viable alternative for NADH regeneration. However, the direct regeneration of NADH on pure, unmodified metallic electrodes results in a very low yield of enzymatically active NADH, which is mostly due to the formation of enzymatically inactive NAD_2 dimer and also to some extent due to

* Corresponding author. Tel.: +1-514-398-4273;
fax: +1-514-398-6678.

E-mail address: sasha.omanovic@mcgill.ca (S. Omanovic).

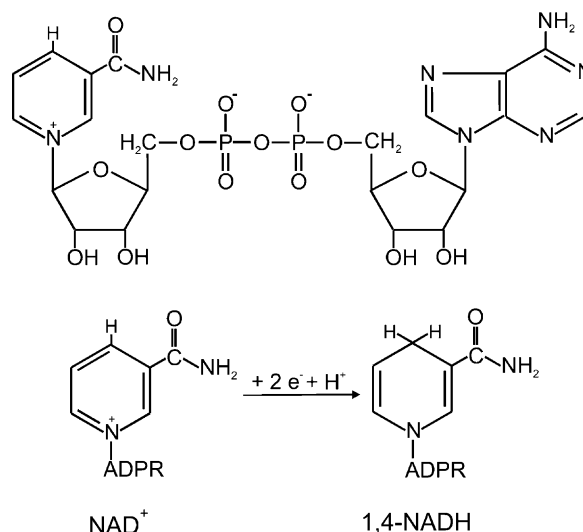
Nomenclature

<i>A</i>	absorption
<i>A</i>	electrode surface area (cm ²)
<i>c</i>	concentration (mol cm ⁻³)
<i>C</i>	capacitance (F cm ⁻²)
CPE	constant phase element (Ω ⁻¹ s ^{<i>n</i>} cm ⁻²)
<i>D</i>	diffusion coefficient (cm ² s ⁻¹)
<i>E</i>	potential (V)
<i>f</i>	frequency (Hz)
<i>F</i>	Faraday constant (96 485 C mol ⁻¹)
<i>j</i>	current density (A cm ⁻²)
<i>k</i>	heterogeneous reaction rate constant (cm s ⁻¹)
<i>k'</i>	homogeneous reaction rate constant (s ⁻¹)
<i>n</i>	number of electrons
<i>n</i>	exponent of a constant phase element
<i>N</i>	number of moles (mol)
<i>Q</i>	charge (C cm ⁻²)
<i>r</i>	reaction rate, mol cm ⁻² s ⁻¹ (heterogeneous), or mol cm ⁻³ s ⁻¹ (homogeneous)
<i>R</i>	standard gas constant (8.314 J mol ⁻¹ K ⁻¹)
<i>R</i>	resistance (Ω cm ²)
sr	scan rate (V s ⁻¹)
<i>t</i>	time (s)
<i>T</i>	temperature (K)
<i>V</i>	volume (m ³)
<i>W</i>	Warburg impedance element (Ω ⁻¹ s ^{1/2} cm ⁻²)
<i>X</i>	conversion (%)
<i>Z</i>	impedance (Ω cm ²)

Greek letters

α	transfer coefficient
α'	partial reaction order with respect to NAD ⁺
β	partial reaction order with respect to H ⁺
ε	extinction coefficient (mol ⁻¹ dm ³ cm ⁻¹)
η	overpotential (V)

the formation of various NADH isomers. This was investigated in detail by Elving et al. [2], who showed that the enzymatically inactive dimer NAD₂ can be only partially protonated and further reduced to both enzymatically active 1,4-NADH and inactive 1,6-NADH at significantly higher cathodic overpotentials [3]. The separation between the current peaks related to the first and second electron transfer is very large on a Hg electrode, i.e. between 500 and 700 mV depending on the conditions applied, which corresponds to a significant energy difference ranging between 48.2 and 67.5 kJ mol⁻¹, thus indicating that the second electron transfer step requires a much larger energy input. However, the polarographic wave of the second reduction step was observed only in the presence of a surface-active electrolyte. A comprehensive study of products formed in the electrochemical reduction of NAD⁺ was done by Jaegfeldt [4], where it was shown that if NAD⁺ is reduced at -1.1 V versus



Scheme 1. Nicotinamide adenine dinucleotide in its oxidized form (NAD⁺), and its reduction to enzymatically active 1,4 NADH. ADPR stands for adenosine diphosphoribose.

SCE on Hg, the yield of the dimer is 90%. The electrolysis of NAD⁺ at -1.8 V versus SCE decreased the amount of formed dimer to 20%, but increased the amount of formed enzymatically inactive 1,6-NADH to 30%.

Due to the low selectivity of bare, unmodified electrodes, the reduction of NAD⁺ (i.e. regeneration of NADH) has also been investigated on chemically modified metallic electrodes. The approach used has been to increase either the kinetics of the second electron transfer and/or protonation, or to prevent dimerization. Most of the studies dealing with this approach have relied on the modification of the electrode by adsorbed organic layers, or by adsorbed/immobilized biological molecules (enzymes, lipids).

A silver electrode modified with covalently adsorbed L-histidine has been recently used [5]. The study showed that this electrode is capable of reducing NAD⁺ to NADH, without the formation of the dimer. In another study [6], the reduction of NAD⁺ was performed using both unmodified and chemically modified gold and platinum electrodes. The gold-amalgam unmodified electrode gave only ca. 10% enzymatically active NADH, while the yield in active NADH increased to 50% when an unmodified platinum surface was used. On the other hand, when the gold-amalgam electrode was chemically modified (with a cholesterol layer), the yield of active NADH increased to ca. 75%. Shimizu et al. [7] immobilized Rh³⁺ ion into a polymeric anion doped-polypyrrole layer formed on the graphite electrode to regenerate NADH. Depending on the anion and polymer used, the yield of enzymatically active NADH ranged from 26 to 51.7%, while the highest NAD⁺ conversion to NADH (both active and inactive) obtained was ca. 50%. Beley and Collin [8] also showed that NAD⁺ could be reduced to enzymatically active NADH when a reticulated vitreous carbon electrode was covered by a layer of polypyrrole rhodium bis-terpyridine.

Due to the problem related to the nonspecificity of unmodified and chemically modified electrodes to NADH regeneration, the enzymatically catalyzed (electro)reduction of NAD^+ has also attracted a considerable attention, for both biosensor development and larger-scale applications (e.g. bioreactors). A number of studies have been reported, and a large majority of them rely on an electron-mediator assisted reduction mechanism. Warriner et al. [9] modified the surface of a platinum electrode with a poly(3-methylthiophene):poly(phenol red) film, which served as an electron mediator for reduction of NAD^+ to NADH. They showed that this configuration, which is developed as a biosensor configuration, is capable of regenerating a certain amount of enzymatically active NADH. Similarly, Karyakin et al. [10] used poly(neutral red)/ NAD^+ /alcoholdehydrogenase/Nafion modified glassy carbon electrode in a biosensor configuration to investigate a possibility of active NADH regeneration. They demonstrated that the detection of acetaldehyde was possible using this electrode, thus showing that the formation of active NADH was achieved. However, in these two papers [9,10] the authors did not report the yield of the active NADH. Fry et al. [11–13] have published a series of papers on the reduction of NAD^+ to NADH on glassy carbon and vitreous carbon electrodes modified by a layer of immobilized methyl viologen and lipoamide dehydrogenase. They showed that the enzyme-catalyzed reduction of NAD^+ on such modified electrodes results in the production of enzymatically active NADH, but the amount of active NADH produced was not explicitly reported. Chen et al. [14] very recently presented their results on the evaluation of in situ electroenzymatic regeneration of NADH in packed bed membrane reactors, where they concluded that the direct electrochemical regeneration of NADH is not feasible in this configuration, but requires the use of methyl viologen and enzyme lipoamide dehydrogenase. They also concluded that the most efficient method is to immobilize the mediator and enzyme on the electrode using Nafion. No information on the amount of active NADH was reported in the paper. An important contribution in this field was also made by Kim et al. [15,16] in their papers that discuss the kinetics of the interaction of methyl viologen and diaphorase enzyme for the electrocatalytic reduction of NAD^+ using a gold-amalgam electrode.

Due to a high specificity of certain enzymes for NADH, the enzymatic regeneration of NADH is a very promising method. However, this approach results in a rather complex electrode system due to difficulties related to immobilization of an enzyme and electron mediator at the electrode surface, loss of the enzyme activity, electron-mediator leakage, and also a rather slow NADH regeneration rate. Therefore, the *direct* electrochemical regeneration of an enzymatically active form of NADH would be a much more desirable method. As already discussed, the use of unmodified metal electrode surfaces does not give promising results due to formation of an inactive dimer in large quantities (50–90%), a result of the slow kinetics of the second reaction step (electron-transfer

and hydrogen addition). As already outlined, this could be, to a certain degree, avoided through the physical prevention of the dimer formation at a molecular level by modifying the electrode surface using self-assembled monolayers [6], or by using an electron mediator incorporated in a conducting polymer film [7,8]. However, it has been shown that these previously used modified electrodes lack long-term stability and durability due to the loss of the modification layer under the applied reduction reaction conditions. Therefore, it would be desirable to design a whole-metallic electrode that would have a long-term stability and offer a high efficiency in reduction of NAD^+ to enzymatically active NADH.

In our previous work, using potentiodynamic and potentiostatic electrochemical techniques, we demonstrated that a glassy carbon electrode modified by a sub-monolayer of ruthenium (RuGC) is capable of reducing NAD^+ directly to NADH, avoiding the formation of dimer NAD_2 [17,18]. It was postulated that Ru sites have a bifunctional role, serving as both proton-providing sites, and as a possible physical barrier for dimerization of NAD-free radicals. A set of kinetic and thermodynamic parameters was calculated and verified independently using various experimental techniques. However, the amount of active 1,4-NADH regenerated using this new electrode was not discussed in the paper, nor was the structure of the electrode/electrolyte interface. Hence, in this paper we report our results on the second phase of the project that focused on the development of an ‘all-solid’ electrode capable of regenerating enzymatically active NADH at a high yield. The paper is divided in four major parts. In the first part initial results on the reduction of NAD^+ on the RuGC electrode will be discussed and compared to pure GC and Ru surfaces, followed by the discussion on the conformational (orientation) behavior of an NAD^+ molecule at the electrode/electrolyte interface. More information on the structure of the electrode/electrolyte interface, obtained on the basis of electrochemical impedance spectroscopy measurements, is presented in the second part of the paper, while the third part of the paper discusses the results of the long-term potentiostatic electrolysis of NAD^+ (i.e. regeneration of NADH) in a batch electrochemical reactor. A detailed kinetic study of the NAD^+ reduction reaction under the potentiostatic conditions applied in the electrolysis is presented in the last part of the paper, and compared with the short-term experiments under the same conditions.

The authors’ hypothesis was that if the rate of the second reduction step (electron and hydrogen transfer) could be enhanced, thus preventing the coupling of free radicals (both by the enhanced hydrogen and electron-transfer kinetic and physical blocking), the dimer formation could be avoided, or at least significantly decreased, resulting in an increased yield of enzymatically active NADH. For that purpose, we modified a glassy carbon (GC) electrode surface by a sub-monolayer of deposited ruthenium (Ru). The GC surface was chosen since it offers a high hydrogen evolution overpotential, a condition necessary in most reduction reactions occurring at potentials more negative than the re-

versible H^+/H_2 couple potential [2]. In addition, the GC surface offers a high stability, reproducibility and, due to its low cost, high suitability for a possible industrial application. On the other side, ruthenium was chosen due to its ability to adsorb hydrogen at low cathodic overpotentials relative to the NAD^+ reduction potential, and also its ability to form a H-Ru bond of an intermediate strength, thus ensuring high coverage with hydrogen at low overpotentials while still allowing it to desorb without investing a considerable amount of energy. This is also the major requirement in electrochemical hydrogen evolution catalysis [19]. As it will be shown, our hypothesis will be proven by demonstrating that the RuGC electrode is indeed capable of reducing NAD^+ directly to NADH at a very high yield (96% under the optimum experimental conditions) of enzymatically active 1,4- NADH .

2. Experimental

The regeneration of NADH from NAD^+ using a Ru-modified GC electrode was studied in 0.05 M phosphate buffer solution at pH 7.0 and temperature of 295 K. The buffer was prepared by dissolving monobasic KH_2PO_4 (Sigma, P-5379) in ultra-pure deionized water (resistivity 18.2 $\text{M}\Omega\text{ cm}$) and adding 0.10 M sodium hydroxide (made from concentrated volumetric solution, ACP Chemical Inc.). An NAD^+ solution was prepared by dissolving a proper amount of $\beta\text{-NAD}^+$ (sodium salt, purity 98%, Sigma N-0632) in 0.05 M phosphate buffer pH 7.0.

A standard three-electrode, two-compartment cell was used in all experiments. The counter electrode was a large-area platinum electrode of high purity (99.99%, Johnson-Matthey), which was degreased by refluxing in acetone, sealed in soft glass, electrochemically cleaned by potential cycling in 0.5 M sulfuric acid, and stored in 98% sulfuric acid. During the measurement, the counter electrode was separated from the main cell compartment by a glass frit. The reference electrode was a commercially available saturated calomel electrode (SCE), to which all potentials in this paper are referred. The working electrode was a Ru-modified glassy carbon electrode (RuGC). Prior to Ru electrodeposition, the surface of the two-dimensional GC electrode was polished with a diamond paste down to 0.03 μm , followed by degreasing with ethanol in an ultra-sound bath and electrochemical activation in 0.5 M H_2SO_4 by potentiodynamic polarization between -1.0 and 1.5 V versus SCE, 40 cycles, scan rate 100 mV s^{-1} . A sub-monolayer of ruthenium was potentiostatically deposited onto the prepared GC electrode at -0.2 V versus SCE from a 1 mM RuCl_3 solution in 0.5 M H_2SO_4 . Fig. 1 shows a scanning electron microscope (SEM) image of a glassy carbon electrode modified by a sub-monolayer of electrodeposited ruthenium (Ru). It can be seen that ruthenium forms well separated and dispersed islands on the electrode surface. The size distribution of Ru islands is rather

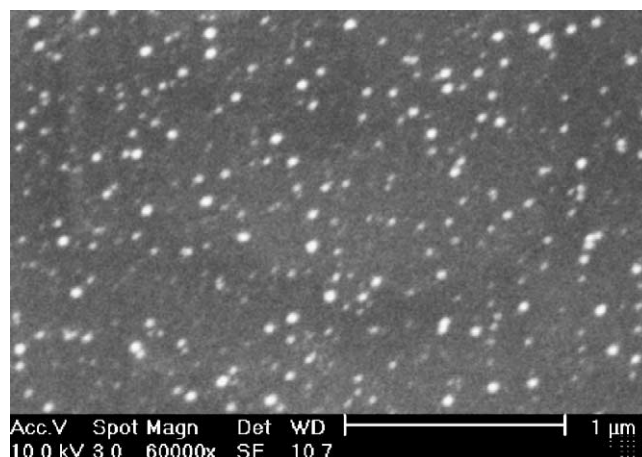


Fig. 1. Scanning electron microscope image of a RuGC electrode surface obtained after electrodeposition of Ru on a freshly prepared and electrochemically activated GC surface.

wide, between ca. 10 and 40 nm, and the separation distance between islands varies from ca. 20 to over 200 nm. From scan-dependent cyclic voltammetry measurements made in the double-layer region in phosphate buffer pH 7.0, the true surface area of RuGC electrodes used in the measurements was estimated [20–22], and the corresponding values reported in this paper are, thus, referred (normalized) to the true surface area of the electrodes used in measurements.

All the measurements were carried out in an oxygen-free solution, which was achieved by continuous purging of the cell with argon gas. Except electrolysis experiments, all other measurements were made in an unstirred (quiescent) solution and the inert atmosphere was maintained by saturating the cell space above the electrolyte with argon. Electrochemical techniques of linear polarization voltammetry, potentiostatic measurements, electrochemical impedance spectroscopy and differential capacitance were employed using an Autolab potentiostat/galvanostat PG-STAT 30, handled by the GPES v. 4.9 software, while the Philips XL-FEG-SEM scanning electron microscope was used for the electrode surface imaging, and Varian UV-Vis spectrophotometer for the qualitative and quantitative measurements of the electrolysis products and activity assays.

The NADH activity tests were made according to the regular Sigma Quality Control Test Procedure (EC 1.8.1.4) using lipoamide dehydrogenase (191 U/mg, Sigma L-2002) as an enzyme and DL-6,8-thioctic acid amide (lipoamide, purity 99–100%, Sigma T-5875) as a substrate.

3. Results and discussion

3.1. Linear polarization voltammetry and capacitance measurements

Fig. 2 shows polarization curves of glassy carbon, ruthenium (Ru) and ruthenium modified glassy carbon (RuGC)

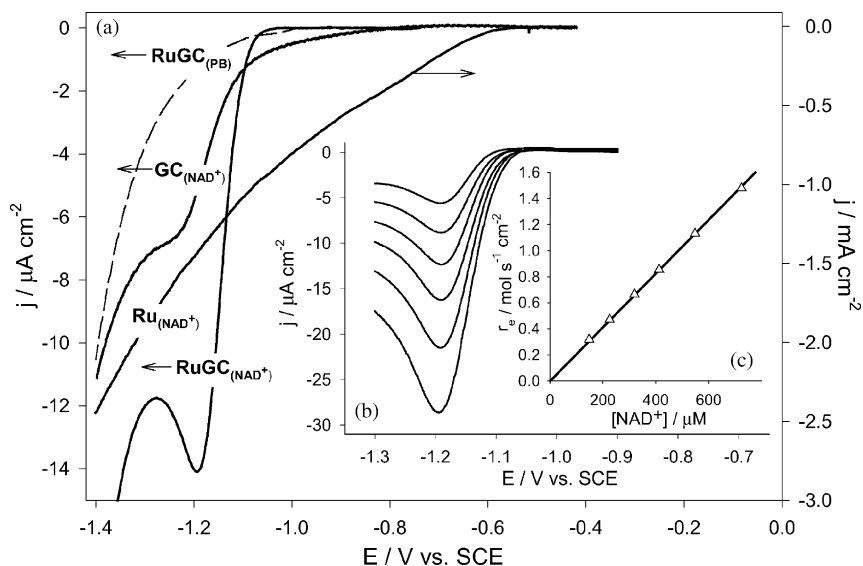


Fig. 2. (a) Cyclic voltammograms of GC, Ru and RuGC electrodes recorded in phosphate buffer pH 7.0 containing 300 μM of NAD^+ (solid lines), and RuGC_(PB) electrode only in phosphate buffer (dashed line). The scan rate, $sr = 100 \text{ mV s}^{-1}$. The curves were normalized for the double-layer charging current. (b) Cyclic voltammograms of a RuGC electrode in phosphate buffer pH 7.0 containing various concentrations of NAD^+ . The concentration increases with the peak current increase as 150, 225, 320, 410, 550, and 725 μM . Scan rate, $sr = 100 \text{ mV s}^{-1}$. The voltammograms were normalized for the background current. (c) Dependence of the electrochemical reaction rate on NAD^+ concentration obtained from the peak current values of voltammograms in (b).

electrodes recorded in a phosphate buffer solution containing 300 μM of NAD^+ . While the NAD^+ reduction peak recorded at ca. -1.20 V is well pronounced on the RuGC electrode, the reduction of NAD^+ on pure GC is rather manifested as a cathodic shoulder. The peak potential recorded on RuGC is in close agreement with the value obtained on a cholesterol-modified gold-amalgam electrode [6], and basal pyrolytic graphite electrode [23]. Our previous work [17,18] showed that the cathodic peak on a RuGC electrode corresponds to the two-electron reduction of NAD^+ to NADH (Scheme 1), while the peak recorded on a bare GC electrode corresponds to the reduction of NAD^+ to free NAD -radical, which involves a transfer of only one electron. Further reduction of the free radical to NADH in the potential window investigated (Fig. 2) is not possible on bare GC due to the rapid formation of dimer NAD_2 [2,24], which is enzymatically inactive. Elving et al. [2] showed that the second cathodic peak (i.e. polarographic wave), that corresponds to the reduction of the free NAD -radical to NADH , could actually be recorded at -1.6 V on a mercury electrode, i.e. ca. 400 mV more negative of NAD^+ reduction peak potential in Fig. 2, but only in the presence of surface-active compounds. While the reduction of NAD^+ is apparent on RuGC and GC, its reduction on the Ru electrode did not result in appearance of any current peak (Fig. 2). Since Ru is a good hydrogen evolution catalyst [19], the current recorded during the cathodic polarization is related mainly to the hydrogen reduction reaction (HER), rather than the NAD^+ reduction. This was also confirmed by a separate experiment in which the electrode was polarized in the same potential region but in an NAD^+ -free solution, and the recorded cur-

rent response was almost identical to the one in Fig. 2. It is evident from Fig. 2 that hydrogen evolution on Ru starts already at -0.5 V , i.e. ca. 700 mV more positive of the NAD^+ reduction peak on RuGC and GC, and at -1.20 V the HER already proceeds at a high rate (note the difference between the two current scales on the graph). However, it is reasonable to expect that NAD^+ reduction is a parallel reaction occurring on Ru in this potential region, but we have not investigated the relative reaction rate ratio between the two competitive reactions.

As we already previously discussed in [17,18], the NAD^+ reduction reaction on RuGC has been shown to be highly irreversible, which can also be seen from the potential difference between the peak position in Fig. 2 and a formal potential for the NAD^+/NADH couple, $E^0 = -0.556 \text{ V}$ versus SCE [2], resulting in an overpotential of more than -600 mV . However, in this paper it is not our intention to evaluate and discuss catalytic properties of the RuGC electrode on the basis of overpotential values, but rather on the basis of the RuGC electrode ability to reduce NAD^+ directly to enzymatically active NADH , instead of the enzymatically inactive NAD_2 , which is obtained by direct reduction on chemically and/or enzymatically unmodified electrodes as discussed previously in the introduction.

Fig. 2 also shows a set of polarization curves recorded at various concentrations of NAD^+ in solution (plot b). The plot demonstrates that the recorded peak current (and corresponding charge) increases with increase in NAD^+ concentration, and the observed dependence presented in Fig. 2c shows very good linearity. This shows that, under the conditions applied in the experiment, the amount of NAD^+

present at the surface at a distance out of the diffusion length is directly proportional to NAD^+ concentration in the bulk electrolyte. The observed proportionality is linear, indicating that the NAD^+ reduction reaction is of first order with respect to NAD^+ . However, the kinetics of the NAD^+ reduction reaction and the linear polarization curves presented in Fig. 2b will be discussed in detail later in the paper alongside a discussion of NAD^+ reduction kinetics.

Using the equation that relates the peak current density to scan rate and concentration [25–27]:

$$j_p = 2.99 \times 10^5 n(\alpha n)^{1/2} c D^{1/2} (\text{sr})^{1/2} \quad (3.1)$$

and noting that in Fig. 2c the reaction rate, r_e , is calculated from the peak current density, j_p , as $r_e = j_p/nF$ [25] the apparent diffusion coefficient value calculated from the slope of line in Fig. 2c is $D = 4.5 \times 10^{-8} \text{ cm}^2 \text{ s}^{-1}$. The transfer coefficient value in Eq. (3.1) was calculated at each NAD^+ concentration from the shape-factor equation, $|E_p - E_{p/2}| = 1.86RT/\alpha nF$ [25], where E_p and $E_{p/2}$ represents the peak and half-peak potential, respectively. The mean value obtained is $\alpha = 0.52 \pm 0.03$. Referring to the reaction Scheme 1, the number of electrons exchanged is 2, and hence, in the above quoted equations, and also in all other equations in the paper in which a number of electrons is used as a required quantity, a value of n is taken to be 2, $n = 2$. The diffusion coefficient value calculated above seems to be rather low for diffusion of NAD^+ in a solution, where a theoretical value of $3.3 \times 10^{-6} \text{ cm}^2 \text{ s}^{-1}$ [17,18] was calculated, and $2.4 \times 10^{-6} \text{ cm}^2 \text{ s}^{-1}$ [28] was measured for NADH diffusion. This indicates that the diffusion of NAD^+ most likely does not occur in the solution, but rather could be considered as the surface diffusion. We discussed this in more detail in

[17,18], where we discussed our results obtained using a number of different experimental techniques and conditions, namely the linear polarization voltammetry with the variable scan rate, differential pulse voltammetry, chronoamperometry and chronopotentiometry. The results of all these experiments gave us the diffusion coefficient value very close to the value reported here, which validates the approach used to determine the diffusion coefficient.

Fig. 3 shows a set of concentration-dependent differential capacitance (DC) curves recorded on a RuGC electrode in the potential region of NAD^+ reduction (the curves were normalized for the differential capacitance response in the absence of NAD^+ in the solution), while the inset to the figure shows raw DC curves recorded in a wide potential region in the NAD^+ -free solution (curve a) and in the solution containing $725 \mu\text{M}$ of NAD^+ (curve e). From the inset it is evident that the capacitance in the potential region between 0 and ca. -1.0 V decreased after the addition of NAD^+ (compare curves a and e) indicating the presence of NAD^+ on the RuGC surface even at high positive potentials. By comparing the DC curves a and e presented in the inset to Fig. 3, it can be seen that the potential-dependent capacitive behavior of the electrode in the potential region between 0 and ca. -1.0 V is not influenced by the presence of adsorbed NAD^+ , i.e. both DC curves show similar potential-dependent behavior (shape). This indicates that the surface arrangement of the adsorbed NAD^+ in this potential window does not change with the change in electrode potential. Elving et al. [2] postulated that in an aqueous (i.e. polar) solution and in the absence of specific enzymes, the NAD^+ molecule (Scheme 1) exists in a folded conformation, which brings the nicotinamide and adenine rings together, with the

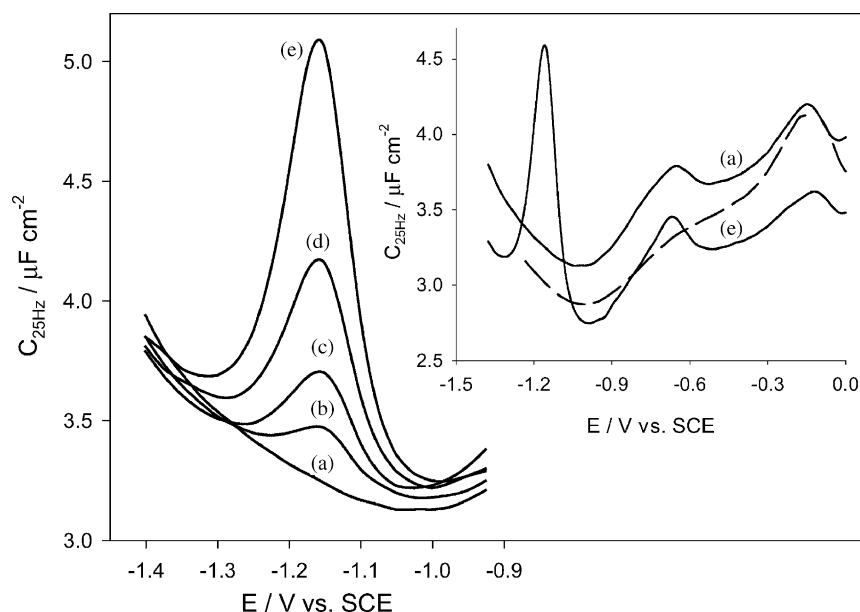


Fig. 3. Differential capacitance curves recorded at 25 Hz in phosphate buffer pH 7.0 containing (a) $0 \mu\text{M}$, (b) $100 \mu\text{M}$, (c) $225 \mu\text{M}$, (d) $410 \mu\text{M}$, and (e) $725 \mu\text{M}$ of NAD^+ . The curves recorded in the NAD^+ solutions were normalized for the capacitance recorded in the phosphate buffer solution. Inset: differential capacitance curves recorded on a RuGC electrode (solid lines) in (a) pure phosphate buffer, and (e) phosphate buffer containing $725 \mu\text{M}$ of NAD^+ . The dashed curve represents the differential capacitance curve recorded on a GC electrode in pure phosphate buffer.

pyrophosphate group as a hinge. They also concluded that both rings are parallel with the electrode surface (Hg in their case), with the adenine ring oriented in a flat position to the surface. Curve a in the inset to Fig. 3 shows the DC behavior of a RuGC electrode in the absence of NAD^+ , while for comparison, a DC curve recorded on bare GC is also presented (dashed curve). The potential-dependant behavior of both electrodes is similar, except around -0.65 V, where the RuGC electrode displays a pronounced capacitive peak. This peak can be related to the presence of Ru-surface sites (see Fig. 1), most likely due to their interaction with hydrogen (i.e. formation of an M–H bond). This is in accordance with the cyclic voltammetry behavior reported in our previous paper (Fig. 2 in [17]). The DC curve a in the inset to Fig. 3 shows that the point-of-zero-charge (pzc) of the RuGC electrode (and also the bare GC electrode) is at ca. -1.05 V versus SCE. Hence, at potentials more positive than the pzc, the RuGC electrode is positively charged, which results in repulsion between a positively charged nicotinamide ring of NAD^+ and the electrode surface, thus facilitating the adsorption of NAD^+ with the orientation of the adenine ring part of NAD^+ towards the surface, as also proposed by Elving et al. [2] in the case of NAD^+/Hg system. Therefore, a long electron-tunneling (or hopping) path between the electrode and the nicotinamide ring could contribute to the sluggish NAD^+ reduction kinetics observed at the formal potential [17,18], i.e. to the fact that a large overpotential (ca. -600 mV) has to be applied in order to reduce NAD^+ at a significant rate. However, at potentials more negative than the pzc, the normalized DC curves in Fig. 3 show a well pronounced DC peak at ca. -1.15 V. The peak value increases with the increase in NAD^+ concentration, and the observed dependence is linear with $R^2 = 0.994$ (graph not shown here). This is in accordance with concentration-dependent linear polarization measurements presented in Fig. 2b. In addition, the potential of DC peaks in Fig. 3 is in the same potential region as the voltammetric peaks presented in Fig. 2b. Taking into account these two last observations (concentration dependence and peak potential position), the DC behavior recorded at potentials more negative than the pzc is related to the onset of reduction of NAD^+ . Hence, it is evident from both Figs. 2 and 3 that an overpotential of ca. -600 mV has to be applied in order to reduce NAD^+ at an appreciable rate. Besides the electrochemical kinetic effect related to the increase in the kinetics of NAD^+ reaction by increasing the overpotential (i.e. lowering of the free energy of activation), an additional effect related to the change in the orientation of the molecule at the surface can be expected to partially contribute to the increased reaction kinetics. Namely, at potentials more negative than the pzc the electrode surface is negatively charged. Therefore, in this potential range, we can expect the NAD^+ molecule to reorient at the surface, now with the positively charged nicotinamide ring oriented towards the negatively charged electrode surface. This would result in the decrease in electron-tunneling distance, which in turn contributes to the increase in the reaction kinetics,

i.e. electron-transfer kinetics. This configuration would also facilitate protonation of the NAD^+ molecule by hydrogen adsorbed at neighboring Ru sites, and thus increase the reaction kinetics (Scheme 1). Hence, it appears that the DC peaks presented in Fig. 3 are related to the reorientation and subsequent reduction of NAD^+ molecules adsorbed on the RuGC surface.

3.2. Electrochemical impedance spectroscopy

The electrochemical impedance spectroscopy (EIS) technique was applied to further investigate the RuGC electrode/electrolyte interface and the corresponding processes that occur on the RuGC surface in the presence of NAD^+ . To ensure complete characterization of the interface and surface processes, EIS measurements were made over six frequency decades, from 50 kHz to 50 mHz at several selected potentials, i.e. in the potential region where NAD^+ reaction does not occur (-0.5 V) and in the NAD^+ reduction potential range (-1.10 and -1.20 V). Fig. 4 shows an example of an EIS spectrum recorded at -1.10 V on a RuGC electrode in a phosphate buffer solution without the presence of NAD^+ (triangles). The presentation of the data in the form of a Bode impedance plot clearly reveals the presence of three distinguishable frequency-dependent segments. Therefore, assuming the presence of two time constants, one of which reflects a mass-transfer controlled response, experimental data were fitted using a nonlinear least-squares fit analysis (NLLS) software [29] and an electrical equivalent circuit (EEC) composed of one (CPE₁R₁)- and one (CPE₂[R₂W])-time constant in parallel (inset to Fig. 4).

In the high-frequency region, the absolute impedance curve (Fig. 4) is almost independent of the frequency, with the phase angle value approaching zero degree. This is a typical response of a resistive behavior and corresponds to the ohmic resistance of the phosphate electrolyte between the working and reference electrode, denoted in the electrical equivalent circuit (EEC, inset to Fig. 4) as R_{el} . In the frequency region between ca. 1 kHz and 100 Hz, a linear relationship can be observed between the absolute impedance and the frequency with a slope of $d\log|Z|/d\log(f) = -0.77$. The phase angle reaches a maximum of ca. -65° , and then starts to decrease at frequencies below ca. 100 Hz, due to the increase in the resistive response related to the charge-transfer kinetics, i.e. resistance R_1 , and also due to the onset of response of a low-frequency (LF) process characterized by a higher time constant (CPE₂[R₂W]). Therefore, the high-frequency region can be related to the fast charging/discharging process at the electrode/electrolyte interface [25,30,31], where CPE₁ represents the capacitance related to the electrode/electrolyte interface, while in the NAD^+ -free solution R_1 represents the charge transfer resistance related to the hydrogen evolution reaction (note a small cathodic current at -1.10 V on RuGC_(PB) curve in Fig. 2a, which is related to hydrogen evolution). At frequencies below ca. 100 Hz, the influence of the second

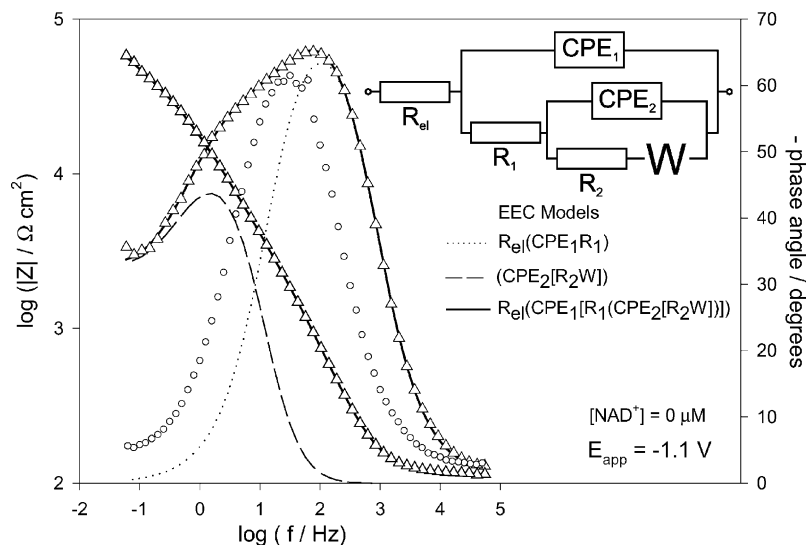


Fig. 4. (Δ) Bode plot of a RuGC electrode recorded at -1.1 V vs. SCE in phosphate buffer pH 7.0. The solid lines represent the simulated spectra obtained using the equivalent electrical circuit model presented as an inset to the figure, while the dashed and dotted lines is the response of the two time constants used to fit the experimental data. (\circ) Bode plot of a bare GC electrode recorded at -1.1 V vs. SCE in phosphate buffer pH 7.0.

time constant ($CPE_2[R_2W]$) starts to appear (Fig. 4), which is characterized with a phase angle shoulder between ca. 10 and 100 Hz, and a change in the slope of the impedance curve toward a lower value ($d\log|Z|/d\log(f) = -0.63$). At frequencies lower than ca. 1 Hz, the phase angle curve approaches ca. -30° , while the impedance curve slope decreases further to $d\log|Z|/d\log(f) = -0.39$, both indicating the response of a mass-transport controlled process [25,30,31]. This is quite in agreement with the observed mass-transport limitations discussed previously in the text (surface-diffusion effect) and also in our previous work [17,18]. Since EIS measurements performed on a pure GC electrode resulted only in one time constant (CPE_1R_1) (see the phase angle plot in Fig. 4, circles), the second time constant ($CPE_2[R_2W]$) observed on a RuGC electrode is, hence, related to the response of Ru sites at the electrode surface. At the moment the origin of the observed mass-transport process is not quite clear to the authors, but since in this potential region Ru sites are already fully saturated with adsorbed hydrogen [32], the recorded mass-transport response could be related to the surface diffusion of hydrogen adsorbed on Ru sites, which has already been discussed in the literature by Brown et al. [33]. The time constant related to this process ($CPE_2[R_2W]$) is characterized by the resistance R_2 , that can be prescribed to the charge transfer resistance at Ru sites, while the constant phase element, CPE_2 , and Warburg impedance element, W , can be related to the Ru sites/electrolyte interfacial capacitance, and mass-transfer impedance, respectively.

In order to investigate the impedance response of each individual time constant separately, and precisely define the corresponding frequency domains, the overall frequency-dependent EIS response was deconvoluted into two observed frequency-dependent regions (i.e. two time

constants), according to the proposed EEC model (inset to Fig. 4). The dotted line in Fig. 4 represents the response of the high-frequency (HF) time constant process, which is characterized by the sub-circuit $R_{el}(CPE_1R_1)$ (due to clarity, only the frequency-dependent variation of the phase angle is presented). It is evident that the modeled sub-spectrum overlaps with the experimental data in the frequency region between ca. 50 kHz and 100 Hz, which shows that in this frequency region the impedance response of the RuGC electrode/electrolyte interface is entirely controlled by the HF time constant process. The impedance response of the second time constant ($CPE_2[R_2W]$) commences at ca. 300 Hz (dashed curve), and at ca. 7 Hz the overall impedance response of the system is characterized by the equal influence of both time constants (phase angle of ca. 32°). However, below 7 Hz the impedance response of the second time constant starts to dominate, while the resistive response of the first time constant reaches a constant value of R_1 . At frequencies between ca. 1 and 2 Hz, the phase angle curve of the second time constant (dashed line) reaches a maximum of 45° , indicating a predominant influence of a mass-transfer process on the overall impedance response [25,30,31]. The summation of the responses of both time constants gives the total response of the system in the whole frequency region (solid curve), which agrees very well with the experimental data (symbols). Hence, the proposed EEC model can be successfully used to model the experimental data and to give a physical picture of the electrode/electrolyte interface and corresponding (surface) charge-transfer and mass-transport processes. The fitting procedure showed that a better agreement between theoretical and experimental data was obtained if a frequency-dependent constant phase element (CPE) was introduced instead of a pure capacitance (C). Generally, use of a CPE is required due to a distribution

of the relaxation times as a result of inhomogeneities present on the microscopic level under the oxide phase and at the oxide/electrolyte interface [30,31]. This may result from contributions from static disorder such as porosity [34], random mixture of conductor and insulator that can be described by the effective medium approximation at percolation [35] or an interface that can be described by either a fractal geometry concept or an RC transmission line concept [36]. The CPE can also include contribution from a dynamic disorder such as diffusion [37]. The impedance of a constant phase element is defined as [29] $Z_{\text{CPE}} = [\text{CPE}(j\omega)^n]^{-1}$, with $-1 \leq n \leq 1$, where Z_{CPE} ($\Omega \text{ cm}^2$) is the impedance of the constant phase element. The constant CPE ($\Omega^{-1} \text{ s}^n \text{ cm}^{-2}$) is a combination of properties related to both the surface and the electroactive species and is independent of frequency. The exponent n is related to a slope of the $\log Z$ against $\log f$ Bode plot, i.e. to the phase angle θ by the relation $n = 2\theta/\pi$ and $j = -1^{0.5}$. A pure capacitance yields $n = 1$, a pure resistance yields $n = 0$, a pure inductance yields $n = -1$, while $n = 0.5$ represents the Warburg impedance.

The use of the CPE in the modeling was also in agreement with the observed deviation in the slope of the impedance curve in the HF region from value -1 ($d\log|Z|/d\log(f) = -0.77$), as well as the deviation of the phase angle (-65°) from value -90° characterized by the response of a perfect capacitor. In addition, the micrograph of the RuGC electrode surface presented in Fig. 1 reveals that the surface is highly inhomogeneous, from morphological, chemical and charge-distribution point of view, thus justifying the use of the CPE instead of the pure capacitance.

Fig. 5 shows the impedance response of the system containing $725 \mu\text{M}$ of NAD^+ in the cell (circles), and for comparison the impedance response of the RuGC electrode

recorded only in a phosphate buffer solution is also presented (triangles). It is evident that the addition of NAD^+ resulted in a significant change in the impedance response. A slight shift of the curves related to the first time constant (HF region) towards higher frequencies indicates a decrease in the CPE_1 value after the addition of NAD^+ , while a considerable difference can be noticed at frequencies below ca. 100 Hz, i.e. in the frequency region related to the charge-transfer and mass-transport processes. The EIS spectrum recorded in the NAD^+ -containing solution is also modeled using the EEC presented in the inset to Fig. 4, and Fig. 5 shows that the agreement between the model (solid curve) and experimental data (circles) is very good, which justifies the use of the proposed model. A visual inspection of the spectra recorded in the presence and absence of NAD^+ in the buffer solution indicates that the addition of NAD^+ produced a decrease of the pseudo-double-layer capacitance (CPE_1) and charge transfer resistance (R_1 and R_2) values. This is more clearly visible in Fig. 6 and Table 1, which represent the dependence of the EEC parameters on NAD^+ concentration. Fig. 6 shows that as the concentration of NAD^+ in solution increases, both resistance values decrease, i.e. inverse of their values R^{-1} increase linearly with concentration. As current is inversely proportional to resistance ($j \propto R^{-1}$) [25] this behavior is quite in agreement with the concentration-dependent linear polarization measurements presented in Fig. 2b, where the peak current also increased linearly with increasing NAD^+ concentration. The charge transfer resistance depends on the number of electrons exchanged in the reduction reaction, and with the NAD^+ concentration increase, a total number of electrons exchanged also increases, and hence R values decrease, i.e. R^{-1} values increase (Fig. 6). Also, the NAD^+ surface

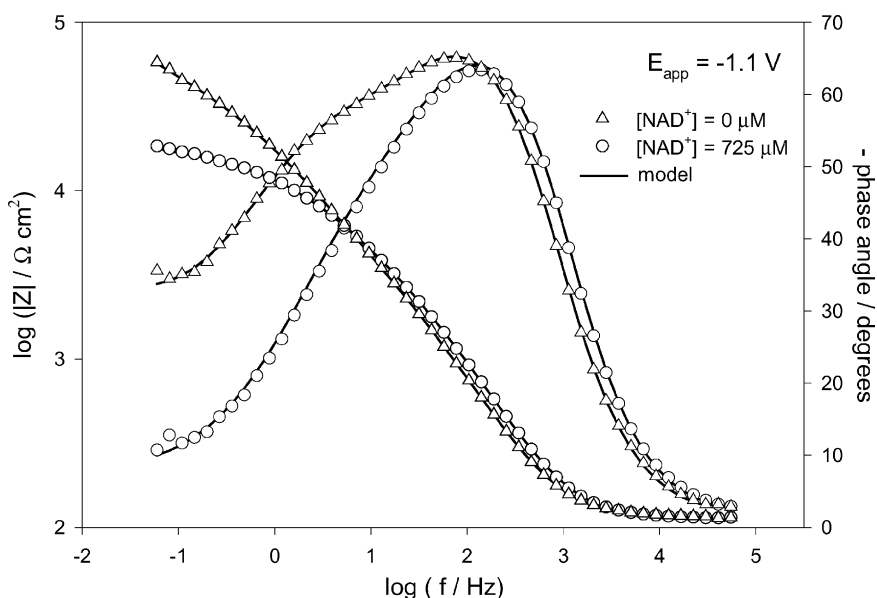


Fig. 5. Bode plots of a RuGC electrode recorded at -1.1 V vs. SCE in phosphate buffer pH 7.0 containing (Δ) $0 \mu\text{M}$ of NAD^+ , and (\circ) $725 \mu\text{M}$ of NAD^+ . The solid lines represent the simulated spectra obtained using the equivalent electrical circuit model presented as an inset to Fig. 4.

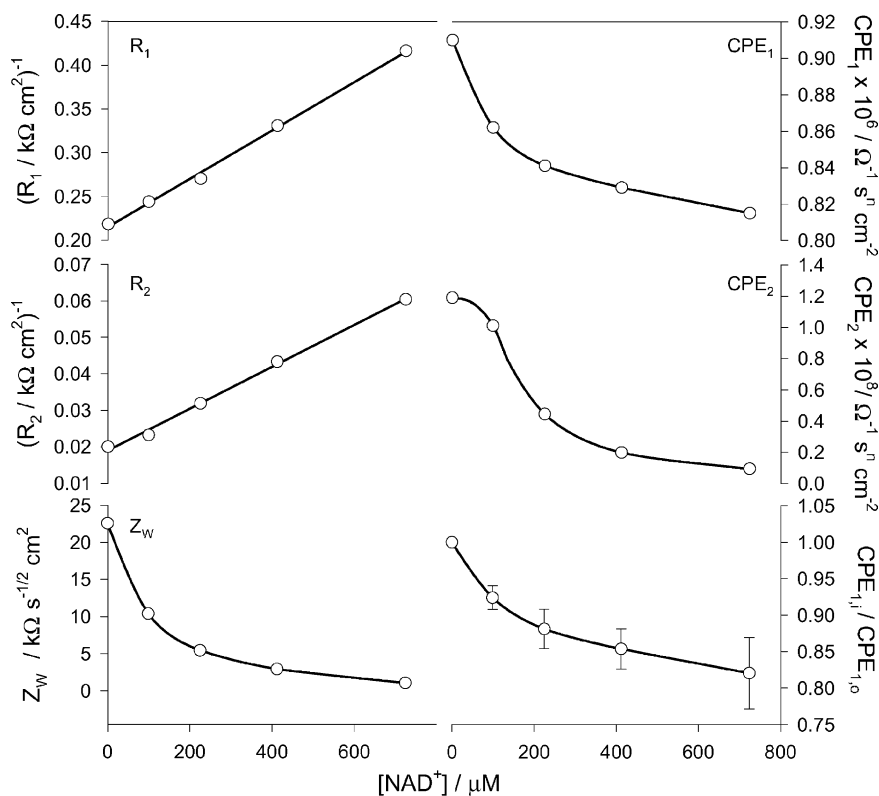


Fig. 6. Dependence of EEC parameter values obtained by fitting the EIS spectra recorded at -1.1 V on NAD^+ concentration in the solution. The graph with error bars shows the relative CPE change recorded at -0.5 , -1.1 and -1.2 V.

mass-transfer flux is directly proportional to the amount of NAD^+ present on the surface at a distance out of the diffusion length, which is in turn directly proportional to NAD^+ concentration in the bulk electrolyte. Hence, similarly to the concentration dependence of R values discussed above, the increase in NAD^+ solution concentration should result in the NAD^+ mass-transfer flux increase, and one

would, therefore, expect to see a decrease in the resistance to mass-transfer. This is the behavior that is actually seen in Fig. 6, which shows that with the increase in NAD^+ concentration in the bulk solution the value of Warburg diffusion impedance Z_W decreases.

The EIS spectra recorded at various NAD^+ concentrations at -1.10 V also show that the value of constant phase

Table 1

EEC parameters obtained by fitting the EIS experimental spectra recorded at various potentials and NAD^+ concentrations in phosphate buffer pH 7.0 using the EEC model presented as an inset to Fig. 4

E_{appl} (V)	$[\text{NAD}^+]$ (μM)	CPE_1 ($\times 10^7 \Omega^{-1} \text{s}^n \text{cm}^{-2}$)	n_1	R_1 ($\text{k}\Omega \text{cm}^2$)	CPE_2 ($\times 10^8 \Omega^{-1} \text{s}^n \text{cm}^{-2}$)	n_2	R_2 ($\text{k}\Omega \text{cm}^2$)	W ($\times 10^5 \Omega^{-1} \text{s}^{1/2} \text{cm}^{-2}$)
-0.5	0	10.20	0.87	6.09	4.13	0.68	140.60	–
	99	9.37	0.87	6.43	2.43	0.66	100.30	–
	225	8.72	0.87	6.75	2.06	0.66	75.82	–
	412	8.39	0.87	6.96	1.96	0.65	97.41	–
	724	7.83	0.87	5.92	0.77	0.61	281.20	–
-1.1	0	9.10	0.89	4.58	1.19	0.63	50.00	4.43
	99	8.62	0.90	4.10	1.01	0.62	43.10	9.62
	225	8.41	0.90	3.70	0.44	0.59	31.41	18.32
	412	8.29	0.91	3.02	0.20	0.55	23.08	34.29
	724	8.15	0.92	2.40	0.09	0.52	16.55	94.85
-1.2	0	9.33	0.89	4.50	2.34	0.66	43.60	4.40
	99	8.57	0.90	4.23	0.47	0.58	35.70	5.78
	225	8.65	0.91	3.47	0.27	0.56	31.20	4.92
	412	8.29	0.91	3.34	0.20	0.55	24.06	5.01
	724	8.14	0.91	2.92	0.17	0.53	19.35	5.95

The spectra recorded at -0.5 V was modeled with the EEC that does not contain the Warburg element.

elements CPE_1 and CPE_2 decrease with increasing NAD^+ concentration (Table 1). Since the CPE_1 and CPE_2 are related to the charging response of the electrode/electrolyte interface of GC and Ru sites, respectively, this indicates that the electrode surface becomes slightly covered with electroactive species having quite different dielectric constant than the solvent (water). EIS measurements performed at higher positive electrode potentials where NAD^+ reduction does not occur (-0.5 V) also generated a similar response (Table 1), which indicates that the species located at the electrode/electrolyte interface are NAD^+ molecules, not the products of NAD^+ reduction reaction, i.e. NADH or possibly NAD_2 . This behavior is quite in agreement with the conclusions obtained from potential-dependent capacitance measurements already discussed previously in the paper (inset to Fig. 3). Fig. 6 also shows a normalized dependence of CPE_1 mean values on NAD^+ solution concentration obtained at the three potentials applied, together with the corresponding standard deviation bars. As discussed above and noticed in Table 1, the behavior of the RuGC electrode/electrolyte interface at various NAD^+ concentrations is similar at all potentials investigated. Table 1 also lists values of the EEC parameters obtained by fitting the EIS spectrum recorded at -1.20 V, and it is quite obvious that the resistive and capacitive behavior of the systems shows the same trend as at -1.10 V.

3.3. Batch electrolysis—regeneration of NADH

In previous work [17,18], using the linear polarization voltammetry experiments, we clearly demonstrated that

the NAD^+ reduction on a RuGC electrode results in the formation of NADH. However, it was not investigated if the formed NADH was of an enzymatically active type, i.e. 1,4-NADH. In order to verify our conclusions based on the potentiodynamic experiments and to investigate if the designed RuGC electrode is capable to produce active 1,4-NADH at a high yield, we performed electrolysis of NAD^+ in a batch electrochemical reactor using a larger area two-dimensional RuGC electrode. The electrolysis was done potentiostatically at several selected potentials in the potential region of the NAD^+ reduction peak in Fig. 2 (between -1.10 and -1.40 V). The amount of NADH produced was monitored at regular time intervals using UV-Vis spectroscopy [4]. Before the electrolysis started, i.e. in a NADH-free solution, the UV-Vis spectroscopy scan gave only one absorbance peak located at 259 nm (not shown here). This is a well-known peak [4] related to the summation of contributions from the nicotinamide and adenine moiety of NAD^+ ($\epsilon_{NAD^+}^{259} = 17\,800\text{ mol}^{-1}\text{ dm}^3\text{ cm}^{-1}$, i.e. $\text{M}^{-1}\text{ cm}^{-1}$). However, as the electrolysis performed at -1.20 V proceeded, a new peak located at 340 nm appeared, the intensity of which increased with time (Fig. 7). This peak is related to the selective absorbance of NADH ($\epsilon_{NADH}^{340} = 6230\text{ mol}^{-1}\text{ dm}^3\text{ cm}^{-1}$), but could also be related to the absorbance of dimer NAD_2 ($\epsilon_{NAD_2}^{340} = 7215\text{ mol}^{-1}\text{ dm}^3\text{ cm}^{-1}$) [4]. Fig. 7b shows the change in relative absorbance at 340 nm with time, and it can be seen that with increase in time the absorbance increases and after ca. 15 h reaches a plateau. Using the above extinction coefficients, the conversion for NAD^+ , X_{NAD^+} [38], was calculated to be ca. 67% after 22 h of electrolysis at -1.20 V versus SCE. Possible

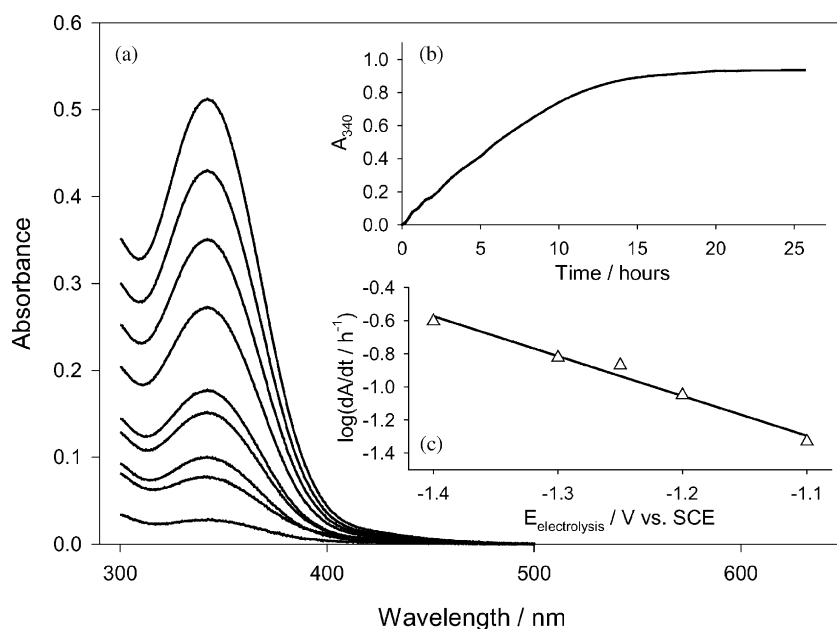


Fig. 7. (a) Absorption spectra recorded at various times during the electrolysis of a $220\ \mu\text{M}$ solution of NAD^+ in phosphate buffer pH 7.0 at -1.2 V vs. SCE. The curves shift to higher absorbance values with increase in time: 20, 40, 60, 90, 120, 180, 240, 310, and 370 min. (b) Time dependence of the absorbance recorded at 340 nm. (c) Dependence of the absorbance-based initial reaction rate derived from the rising portion of absorbance–time curves at short times (dA/dt) on the electrolysis potential $E_{\text{electrolysis}}$.

reasons for not obtaining higher conversion, i.e. for the appearance of the absorbance plateau (Fig. 7b) could be due to a decrease in the electron-transfer driving force (i.e. overpotential) with the decrease in $[\text{NAD}^+]/[\text{NADH}]$ ratio [39].

In order to get preliminary information of the influence of regeneration potential on regeneration reaction rate, the initial regeneration rate based on the measured absorbance change (dA/dt) was determined from the initial slope of an A_{340} versus time curve obtained at each electrolysis potential, and the result is presented in Fig. 7c as a logarithmic dependence. It is obvious that with the increase in electrolysis overpotential, the logarithm of initial regeneration rate linearly increases, which is also predicted by the electrochemical theory of electron transfer [25]. However, we will also see later in the text that although the increase in regeneration overpotential has a positive effect on the regeneration rate increase (Fig. 7c), the actual yield of enzymatically active form of NADH depends significantly on the overpotential applied, and that the highest yield was obtained at -1.20 V. Therefore, further in the text most of the results discussed will be referred and compared to this regeneration potential.

As we previously stated, the absorption peak at 340 m could be related to both NADH and NAD_2 [4]. In order to investigate the amount of enzymatically active 1,4-NADH formed by potentiostatic electrolysis of NAD^+ (Fig. 7), an activity assay was performed according to the procedure described in the experimental part of the manuscript. The assay of the final solution obtained by electrolysis at -1.20 V showed that 96% of the converted NAD^+ was enzymatically active 1,4-NADH. The remaining 4% could be both inactive NADH isomers or/and dimer NAD_2 . The yield of enzymatically active 1,4-NADH obtained at -1.20 V using our RuGC electrode is very high considering that the direct regeneration method was applied and the electrode surface was not chemically modified (with organic assembled layers). By comparison, when a gold-amalgam unmodified electrode is used [6], only ca. 10% of enzymatically active NADH was obtained, while the yield in active NADH increased to 50% when an unmodified platinum electrode was used. If the gold-amalgam electrode was modified with a cholesterol layer, the yield of active NADH increased to maximum ca. 75%. Also, when a pure platinum electrode was used in a NADH regeneration cell modified with an anion-charged membrane as a diaphragm, the yield of enzymatically active NADH ranged from ca. 50% at higher regeneration overpotentials up to ca. 65% at lower regeneration overpotentials [40].

Table 2 shows the yield (in percent) of enzymatically active 1,4-NADH formed at various electrolysis potentials. It can be seen that the optimum electrolysis potential is around -1.20 and -1.25 V, where the highest yields of regenerated 1,4-NADH were obtained (96 and 92%, respectively). However, when the regeneration of NADH was performed at lower potentials, i.e. -1.10 V, the yield of enzy-

Table 2

Percentage of enzymatically active 1,4-NADH regenerated at various electrolysis potentials

$E_{\text{electrolysis}}$ (V) vs. SCE	-1.10	-1.20	-1.25	-1.30	-1.40
Activity of NADH (%)	65	96	92	41	14

Starting NAD^+ concentration was $220 \mu\text{M}$ in phosphate buffer pH 7.0.

matically active 1,4-NADH was lower, 65%, compared to the situation at -1.20 and -1.25 V. Remembering that the kinetics of the second electron transfer to the NAD-radical is much slower than the transfer of the first electron to NAD^+ [1–3], the reason for the lower amount of enzymatically active 1,4-NADH formed at lower overpotentials might be due to the decrease in the rate of second electron transfer at a decreased overpotential, which then, therefore, increases a probability for the dimer formation. On the other hand, the yield of enzymatically active 1,4-NADH obtained by electrolysis at higher overpotentials was even lower, 41% at -1.30 V and 14% at -1.40 V (Table 2). After the completion of electrolysis at these two high overpotentials the measured pH of the solution was above 11. On the other hand, at -1.25 , -1.20 and -1.10 V pH of the solution did not change in the time interval of the experiments. The reason for the observed pH increase at high regeneration overpotentials (-1.30 and -1.40 V) is the hydrogen evolution, which is a reaction that occurs in parallel with the NAD^+ reduction reaction at the RuGC electrode at these high overpotentials (note hydrogen evolution cathodic current at -1.30 and -1.40 V on $\text{RuGC}_{(\text{PB})}$ curve in Fig. 2). Thus, the current efficiency for the NAD^+ reduction is significantly lower compared to the electrolysis performed at the lower three potentials. Experiments performed in our laboratory have shown [17,18] that the NAD^+ reduction reaction is pH independent in the pH range from 5.5 to 10.2, which is due to the adsorption and subsequent supply of the proton participating in the NAD^+ reduction reaction by Ru sites on the RuGC electrode surface. The conclusions obtained were based on the fast potentiodynamic experiments (linear polarization voltammetry and differential pulse voltammetry), while the electrolysis of NAD^+ presented here was done potentiostatically for a prolonged time (24 h). Chenault and Whitesides [1] have reported that the stability of NADH is higher at higher pH values, and hence, the spontaneous decomposition of regenerated NADH could be dismissed as a possible reason for the low yield of 1,4-NADH obtained by electrolysis at -1.30 and -1.40 V. On the other hand, Jaegfeldt [41] has noticed that the amount of active 1,4-NADH produced by electrolysis of NAD^+ at -1.8 V versus SCE using a mercury electrode decreased from ca. 63% at pH 7 down to 50% at pH 10, while at the same time the amount of inactive 1,6-NADH doubled from ca. 15–30%. The amount of the dimer remained constant at about 20% in the entire pH range studied. At the moment, the authors of this paper do

not have any explicit explanation that could be used to justify the low yield of 1,4-NADH obtained at -1.30 and -1.40 V. However, based on the findings reported in Jaegfeldt's paper [41] we could also assume that the significant increase in pH (above 11) recorded during the electrolysis of NAD^+ on RuGC at -1.30 and -1.40 V facilitates the formation of inactive 1,6-NADH instead of active 1,4-NADH, which is opposite to the situation recorded at lower overpotentials. Yun et al. [40] have also reported that the amount of enzymatically active 1,4-NADH regenerated using a platinum electrode and a cell modified with an anion-charge membrane depends on the electrolysis overpotential applied. They have related the lower yield of 1,4-NADH obtained at higher overpotentials to the formation of the dimer. A possibility of inactive 1,6-NADH formation has not been discussed in their paper, and no information about a possible change in the pH of solution at higher overpotentials has been reported.

3.4. Kinetics of NAD^+ reduction

Our previous results [17,18] demonstrated that the NAD^+ reduction reaction performed under the potentiodynamic conditions (linear polarization voltammetry and differential pulse voltammetry measurements) is of first order with respect to NAD^+ and zero order with respect to the proton. In this section of the paper we are going to present the kinetics analysis related to the NAD^+ reduction reaction on the basis of experiments performed under the potentiostatic conditions.

Fig. 8 shows the dependence of NAD^+ concentration on time obtained by the reduction of NAD^+ at a constant poten-

tial of -1.20 V. Since our detailed study reported in [17,18] has shown that the NAD^+ reaction is of zero order with respect to proton, the reaction rate for the reaction in Scheme 1, r_{NAD^+} ($\text{mol cm}^{-3} \text{s}^{-1}$), can be written as [42,43]:

$$\begin{aligned} r_{\text{NAD}^+} &= \frac{d[\text{NAD}^+]}{dt} = \frac{1}{V} \frac{dN_{\text{NAD}^+}}{dt} \\ &= -k'_{\text{NAD}^+} [\text{NAD}^+]^{\alpha'} \end{aligned} \quad (3.2)$$

where k'_{NAD^+} ($\text{cm}^3 \text{mol}^{-1}$) $^{\alpha'-1} \text{s}^{-1}$ is the homogeneous reaction rate constant with respect to the rate of change in the concentration of $[\text{NAD}^+]$ (mol cm^{-3}), N_{NAD^+} the number of moles of NAD^+ reacted in a unit reactor volume V (cm^3), and α' the partial reaction order with respect to NAD^+ . However, since the investigated reaction is a heterogeneous reaction occurring at the electrode surface (at a constant potential), the rate of the reaction depends on the electrode surface area A (cm^2) and, hence, it would be more appropriate to express the reaction rate and corresponding coefficient in terms of the rate of change of moles of NAD^+ per unit surface area of the electrode ($\text{mol cm}^{-2} \text{s}^{-1}$), rather than per unit volume of the solution ($\text{mol cm}^{-3} \text{s}^{-1}$). This basis is more appropriate for heterogeneous reactions [43]. Hence, this modified rate law for the system investigated can be written as

$$r_{\text{het,NAD}^+} = \frac{1}{A} \frac{dN_{\text{NAD}^+}}{dt} = -k_{\text{NAD}^+} [\text{NAD}^+]^{\alpha'} \quad (3.3)$$

where k_{NAD^+} ($\text{cm}^3 \text{mol}^{-1}$) $^{\alpha'-1} \text{cm s}^{-1}$ is the heterogeneous reaction rate constant. If we take the value of reaction order α' to be 1, which is based on both the experiments reported in [17,18] and the experiments that will be discussed later in the text (Fig. 9), we can integrate the above equation taking

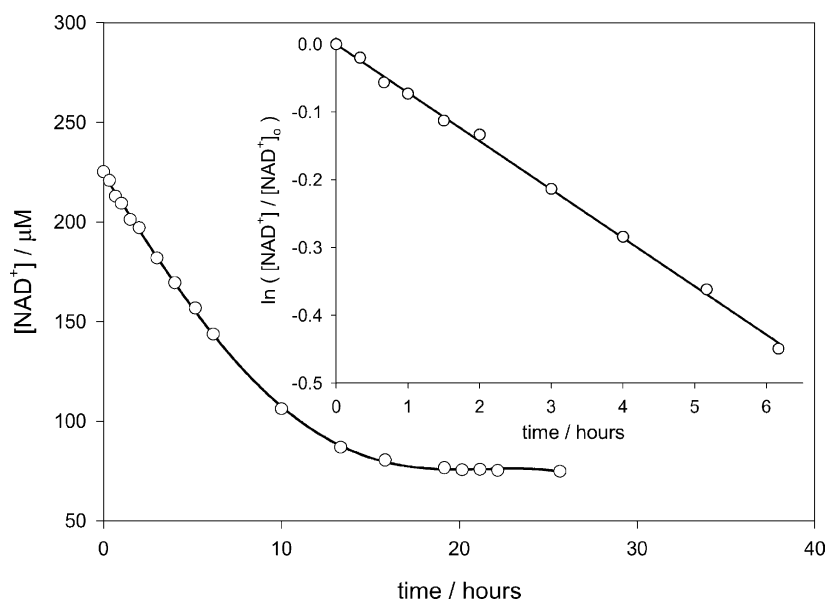


Fig. 8. Time dependence of NAD^+ concentration obtained from the electrolysis experiments performed at -1.2 V (Fig. 7). Inset: the NAD^+ concentration vs. time dependence from the main figure transformed in order to evaluate the reaction rate constant k_{NAD^+} .

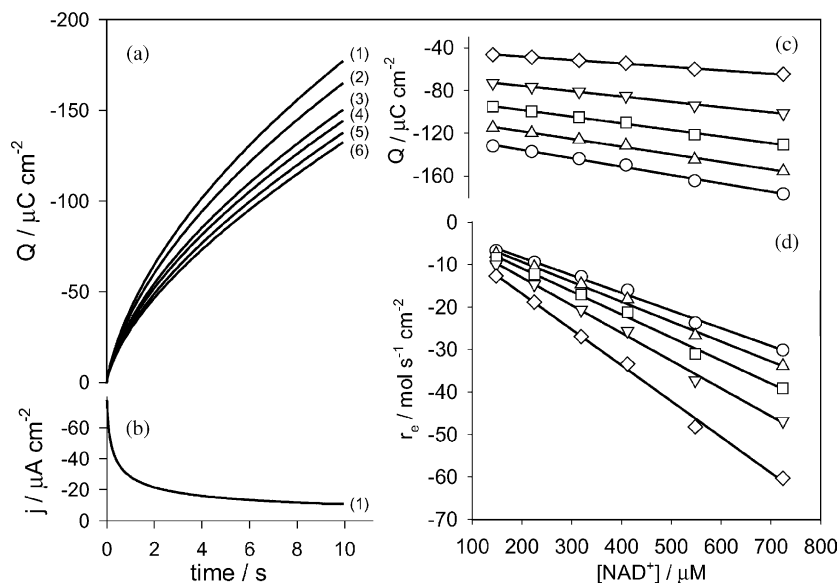


Fig. 9. (a) Chronocoulometric curves recorded at -1.2 V in a phosphate buffer solution containing various concentration of NAD^+ : (1) $725 \mu\text{M}$, (2) $550 \mu\text{M}$, (3) $410 \mu\text{M}$, (4) $320 \mu\text{M}$, (5) $225 \mu\text{M}$ and (6) $150 \mu\text{M}$. (b) Chronoamperometric curve recorded at -1.2 V in solution (1). (c) Dependence of the cumulative charge on NAD^+ concentration obtained from (a) at several selected times: (\circ) 10 s, (Δ) 8 s, (\square) 6 s, (∇) 4 s and (\diamond) 2 s. (d) Dependence of the electrochemical reaction rate on NAD^+ concentration calculated from curves presented in (a) at several selected times: (\circ) 10 s, (Δ) 8 s, (\square) 6 s, (∇) 4 s and (\diamond) 2 s.

the initial state to be at time zero, i.e. before electrolysis, to obtain [38,43]:

$$\ln \frac{N_{\text{NAD}^+}}{(N_{\text{NAD}^+})_0} = \ln \frac{[\text{NAD}^+]}{[\text{NAD}^+]_0} = -k_{\text{NAD}^+} \frac{A}{V} t \quad (3.4)$$

where $(N_{\text{NAD}^+})_0$ represents the number of moles of NAD^+ present in the solution of volume V before the electrolysis, i.e. the initial NAD^+ concentration $[\text{NAD}^+]_0$ at time zero. Note that since the volume of electrolyte solution does not change during the electrolysis, the left-hand side of Eq. (3.4) (presented in terms of mol-ratios) can be expressed as concentration ratios. Hence, if the reaction of NAD^+ reduction is of first-order, equation (3.4) shows that a plot of $\ln([\text{NAD}^+]/[\text{NAD}^+]_0)$ versus t should give a straight line of slope $A/V \times k_{\text{NAD}^+}$. Indeed, when the electrolysis data presented in Fig. 8 (main plot) are transformed in accordance with Eq. (3.4), a linear relationship between $\ln([\text{NAD}^+]/[\text{NAD}^+]_0)$ and time is obtained for the times corresponding to the NAD^+ conversion values up to 36% (first 6 h of electrolysis, inset to Fig. 8). The agreement between the experimental data (symbols) and the model (line) for the first-order reaction kinetics, Eq. (3.4), is quite in accordance with the conclusions obtained on the basis of linear polarization voltammetry (LPV) and differential pulse voltammetry (DPV) results presented in [17,18], where the true partial reaction order with respect to NAD^+ was determined to be 0.99 and 1.00 for LPV and DPV measurements, respectively. Now, from the slope of the line (inset to Fig. 8) the apparent heterogeneous reaction rate constant k_{NAD^+} was calculated to be $3.4 \times 10^{-5} \text{ cm s}^{-1}$. It should be emphasized that the reaction rates and corresponding constants in

Eqs. (3.3) and (3.4) are potential-dependent [25], and as we have seen from the initial kinetics analysis based on the absorbance (Fig. 7c), both should increase with the increase in reduction overpotential. The above k_{NAD^+} value is relatively low, indicating that the overall kinetics of NAD^+ reduction reaction is slow under the experimental conditions applied. However, if we compare our k_{NAD^+} value to the value calculated from the data presented in [44], $2.8 \times 10^{-6} \text{ cm s}^{-1}$ (assuming the first-order kinetics), we can see that our value is an order of magnitude higher.

Further, using this reaction rate constant value and the relation for the half-life for the first-order reaction obtained from Eq. (3.4), $A/V \times k_{\text{NAD}^+} \times t_{1/2} = 0.693$ [38,42,43], the half-life value for the NAD^+ reduction reaction was calculated to be 9.7 h. This value is in agreement with the value that can also be determined from the curve on the main plot in Fig. 8.

Although both the electrolysis data discussed above and the linear polarization voltammetry and differential pulse voltammetry data presented in [17,18] showed that the NAD^+ reduction reaction is of first order with respect to NAD^+ , chronocoulometry measurements were completed to further verify the kinetics parameters obtained on the basis of electrolysis and potentiodynamic data. Fig. 9a shows a set of chronocoulometric curves recorded at -1.20 V at various initial concentrations of NAD^+ , while the curve on Fig. 9b represents the potentiostatic current transient recorded at -1.20 V in quiescent phosphate buffer solution containing $725 \mu\text{M}$ of NAD^+ . The shape of the current transient curve demonstrates that the NAD^+ reduction reaction is purely under the diffusion control, i.e. it obeys

the Cottrell equation [25], as already observed from the EIS measurements discussed previously in the paper, and dc measurements reported in [17]. The current approaches a quasi-constant value after ca. 10 s from the start of the potentiostatic pulse. The chronocoulometric transients in Fig. 9a show that with the increase in NAD^+ concentration the charge related to NAD^+ reduction also increases in the entire time interval region. This is clearly illustrated in Fig. 9c which shows the dependence of cumulative charge measured at various times on NAD^+ concentration. In all cases the relationship is highly linear and the lines are almost parallel. Using the electrochemical definition for the reaction rate, r_e ($\text{mol s}^{-1} \text{cm}^{-2}$) [25]:

$$r_e = \frac{1}{A} \frac{dN_{\text{NAD}^+}}{dt} = \frac{j}{nF} = \frac{Q}{tmF} = -k_{e,\text{NAD}^+} [\text{NAD}^+]^{\alpha'} \quad (3.5)$$

where j represents the current density (A cm^{-2}), n the total number of electrons exchanged in the reaction ($n = 2$), and Q the cumulative charge density (C cm^{-2}) measured at time t (s), we can calculate the reaction order with respect to NAD^+ and the apparent *electrochemical* heterogeneous rate constant, k_{e,NAD^+} (cm s^{-1}), from the data presented in Fig. 9a. It should be noted that the electrochemical and heterogeneous rate constants have the same meaning, but different terms are used in order to distinguish between the experimental methods and quantities used to calculate the constants. The $\ln r_e$ versus $\ln[\text{NAD}^+]$ plots of the data taken (Fig. 9a) at various times gave straight lines (the graph is not shown here but the regression coefficient was $R^2 = 0.996 \pm 0.002$). The mean value of the pseudo-reaction order calculated at 2, 4, 8 and 10 s is 0.98 ± 0.01 , which is in agreement with both the value obtained from the electrolysis experiment (Fig. 8) and potentiodynamic measurements reported in [17,18], and clearly shows that the NAD^+ reduction reaction is of first order with respect to NAD^+ . In cases where diffusion limitations are present (like in the NAD^+ reduction potential region investigated here), the measurement of the *true* reaction rate could be affected. In that case, Fogler [38] relates an apparent reaction order, α'_{app} , to true reaction order, α' , as $\alpha'_{\text{app}} = (1 + \alpha')/2$. However, when comparing the α'_{app} value calculated from the results in Fig. 9 ($\alpha'_{\text{app}} = 0.98$) to the α' value calculated using Fogler's approach ($\alpha' = 0.96$), we can see that the difference between them is insignificant.

Now, having the partial reaction order value known we can calculate the apparent heterogeneous electrochemical reaction rate constant k_{NAD^+} using the rate equation (3.5). Fig. 9d shows the relationship between the electrochemical reaction rate and NAD^+ concentration evaluated at 2, 4, 8 and 10 s, and it is obvious that the observed relationship is highly linear for all times. From the slopes of the lines the apparent heterogeneous electrochemical reaction rate constant was calculated at the selected times and the values are presented in Table 3. The table shows that the apparent heterogeneous electrochemical reaction rate constant value

Table 3

Apparent electrochemical heterogeneous reaction rate constants calculated from chronocoulometric transients in Fig. 9a at various times

Time (s)	2	4	6	8	10
k_{e,NAD^+} ($\times 10^5 \text{ cm s}^{-1}$)	8.44	6.53	5.44	4.69	4.17

depends on time at short reaction times investigated (≤ 10 s). This is quite reasonable to expect since the NAD^+ reduction reaction is surface-diffusion controlled in the potential region investigated (Fig. 9b and Refs. [17,18]), and since it usually takes approximately 10 s to develop a quasi-constant concentration gradient in an unstirred solution, after which the reaction rate, i.e. current, practically remains constant at a fixed bulk reactant concentration. It has to be noted that the calculated apparent heterogeneous electrochemical reaction rate constant k_{e,NAD^+} is the value related not only to the *electron-transfer* rate, but should be regarded as an apparent electrochemical reaction rate constant which involves both the electron-transfer and surface-diffusion rate. The modeling of cyclic voltammetry curves recorded at various scan rates and NAD^+ concentrations enabled us to calculate the true heterogeneous electron-transfer rate constant at -1.20 V, and the value obtained is $k_{\text{et}} = 4.85 \text{ cm s}^{-1}$ [17,18], which is five orders of magnitude higher than the k_{e,NAD^+} value obtained from chronocoulometric experiments (Table 3). However, this is quite reasonable knowing that the reduction of NAD^+ on a RuGC electrode at -1.20 V is a mass-transport (surface-diffusion) controlled reaction characterized by a low diffusion coefficient value ($4.5 \times 10^{-8} \text{ cm}^2 \text{ s}^{-1}$), as it was already discussed earlier in this paper and in [17,18]. Using the values of apparent heterogeneous electrochemical reaction rate constant, k_{e,NAD^+} and the true heterogeneous electron-transfer rate constant, k_{et} , one can calculate the corresponding ratio between the kinetically controlled current, $j_k = nFck$, and diffusional controlled current, $j_d = nFc(D/\pi t)^{1/2}$ [25]. If 10 s as an upper limit to establish a quasi-state surface concentration gradient is used (Fig. 9b) [25], the calculated ratio is $j_k/j_d = 1.29 \times 10^5$. The ratio between the corresponding electrochemical heterogeneous electron-transfer and apparent reaction-rate constants (Table 3, 10 s) is very close to this value, $k_{\text{et}}/k_{e,\text{NAD}^+} = 1.16 \times 10^5$, and shows that the contribution to the observed difference comes from the slow surface mass-transport process.

Similarly to the chronocoulometry results (Fig. 9), the linear polarization measurements performed in the same concentration region (Fig. 2b) show that the NAD^+ reduction current and corresponding charge (i.e. peak area) increase with increasing NAD^+ concentration in the solution. Using Eq. (3.5) and the polarization curves presented in Fig. 2b, the logarithm of peak current versus logarithm of NAD^+ concentration dependence ($\log j_p$ versus $\log[\text{NAD}^+]$) plot gave a very straight line ($R^2 = 0.9999$) of slope 0.99, thus showing that the reaction is of first order with respect to NAD^+ , which is in agreement with the electrolysis and chrono-

coulometry kinetics data discussed previously in the paper. The r_e versus $[\text{NAD}^+]$ dependence presented in Fig. 2c shows that the agreement between the experimental values and Eq. (3.5) for $\alpha' = 1$ is very good, and from the slope of the line the heterogeneous electrochemical reaction rate constant was calculated to be $k_{e,\text{NAD}^+} = 2.0 \times 10^{-5} \text{ cm s}^{-1}$, a value very close to those obtained from electrolysis experiment ($3.4 \times 10^{-5} \text{ cm s}^{-1}$) and chronocoulometry experiments (Table 3).

4. Conclusions

The regeneration of NADH in a batch electrochemical reactor using a ruthenium modified glassy carbon electrode (RuGC), the structure of the RuGC electrode/electrolyte interface in the presence of NAD^+ in the solution, and the kinetics of NAD^+ reduction on RuGC was investigated in a phosphate buffer solution pH 7.0 using electrochemical techniques of dc linear potential (LP) and constant potential (CA) polarization, ac differential capacitance, and electrochemical impedance spectroscopy. It was shown that the modification of GC by a sub-monolayer of Ru can provide an electrode surface that is, under optimized conditions, capable of reducing NAD^+ directly to NADH, while practically avoiding the formation of the dimer. The results showed that the reduction reaction is highly irreversible, occurring at high cathodic overpotentials (ca. -0.576 V). It was postulated that a large electron-tunneling distance between the electrode and nicotinamide ring of an NAD^+ molecule could be one of the reasons for the high energy requirement for the electron transfer (high overpotential). With the reorientation of the molecule at the electrode surface, caused by the change in polarity of the electrode at potentials negative of the pzc, the electron-tunneling path decreases, which also contributes to the faster electron-transfer kinetic and the reduction of NAD^+ at significant current densities. It was also determined that the NAD^+ reduction reaction is entirely surface mass-transport controlled in the potential region below ca. -1.1 V . EIS measurements showed that the electrode/electrolyte interface and the corresponding charge- and mass-transfer processes can be described by an electrical equivalent circuit composed of two time constants in parallel, with the additional contribution of a mass-transport element (i.e. Warburg impedance). The time constant recorded at higher frequencies can be prescribed to the response of a GC part of the electrode surface, while the lower-frequency time constant can be related to the response of Ru sites on the electrode surface.

The electrolysis of NAD^+ (i.e. regeneration of NADH) in a batch electrochemical reactor at -1.2 V showed that the RuGC electrode is capable of regenerating enzymatically active 1,4-NADH at a high yield (96%). It was shown that the pseudo-reaction rate (based on the absorbance) depends linearly on the applied electrolysis overpotential, and increases with the increase in overpotential. The electrolysis at lower

overpotentials resulted in a lower yield of active NADH, most likely due to the decrease in the electron-transfer kinetic, which enabled the formation of inactive dimers. On the other hand, at high overpotentials the current efficiency for NADH regeneration was rather low due to the hydrogen evolution, and the amount of active NADH formed was also low.

The kinetic analysis was performed using both long-term (electrolysis) and short-term (chronocoulometry) potentiostatic measurements, and fast potentiodynamic measurements (linear polarization). A very good agreement between the apparent heterogeneous reaction rate constant values calculated using the three techniques was obtained, which verifies the approach used in the kinetics analysis. It was shown that the NAD^+ reduction reaction is of first order with respect to NAD^+ . The calculated apparent heterogeneous reaction rate constant values are rather low, which is due to the slow mass-transport of electroactive species at the electrode surface.

Acknowledgements

Grateful acknowledgment is made to the Natural Science and Engineering Research Council of Canada and the Centre for Biorecognition and Biosensors at McGill University for support of this research.

References

- [1] H.K. Chenault, G.M. Whitesides, *Appl. Biochem. Biotechnol.* 14 (1987) 147.
- [2] P.J. Elving, W.T. Bresnahan, J. Moiroux, Z. Samec, *Bioelectrochem. Bioenergy* 9 (1982) 365.
- [3] J. Moiroux, S. Deycard, T. Malinski, *J. Electroanal. Chem.* 194 (1985) 99.
- [4] H. Jaegfeldt, *Bioelectrochem. Bioenergy* 8 (1981) 355.
- [5] Y.-T. Long, H.-Y. Chen, *J. Electroanal. Chem.* 440 (1997) 239.
- [6] S.H. Baik, C. Kang, I.C. Jeon, S.E. Yun, *Biotechnol. Tech.* 13 (1999) 1.
- [7] Y. Shimizu, A. Kitani, S. Ito, K. Sasaki, *Denki Kagaku* 61 (1993) 872.
- [8] M. Beley, J.-P. Collin, *J. Mol. Catal.* 79 (1993) 133.
- [9] K. Warriner, S. Higson, P. Vadgama, *Mater. Sci. Eng. C* 5 (1997) 91.
- [10] A.A. Karyakin, O.A. Bobrova, E.E. Karyakina, *J. Electroanal. Chem.* 399 (1995) 179.
- [11] A.J. Fry, S.B. Sobolov, M.D. Leonica, K.I. Voivodov, *Tetrahedron Lett.* 35 (1994) 5607.
- [12] K.I. Voivodov, S.B. Sobolov, M.D. Leonida, A.J. Fry, *Bioorg. Med. Chem. Lett.* 5 (1995) 681.
- [13] S.B. Sobolov, M.D. Leonida, A. Bertoszko-Malik, K.I. Voivodov, F. McKinney, J. Kim, A.J. Fry, *J. Org. Chem.* 61 (1996) 2125.
- [14] X. Chen, J.M. Fenton, R.J. Fisher, R.A. Peattie, *J. Electrochem. Soc.* 151 (2004) E56.
- [15] S. Kim, S.-E. Yun, C. Kang, *Electrochem. Comm.* 1 (1999) 151.
- [16] S. Kim, S.-E. Yun, C. Kang, *J. Electroanal. Chem.* 465 (1999) 153.
- [17] F. Man, S. Omanovic, *J. Electroanal. Chem.*, 568c (2004) 301.
- [18] S. Omanovic, F. Man, B. Théorêt, W.A. Brown, *Proceedings of the 39th IUPAC Congress and 86th Conference of the Canadian Society for Chemistry*, Ottawa, Ont., Canada, 2003.

- [19] J.M. Jaksic, N.M. Ristic, N.V. Krstajic, M.M. Jaksic, *Int. J. Hydrogen Energy* 23 (1998) 1121.
- [20] R. Gonzalez-Cruz, O. Solorza-Feria, *J. Solid State Electrochem.* 7 (2003) 289.
- [21] W. Sugimoto, T. Kizaki, K. Yokoshima, Y. Murakami, Y. Takasu, *Electrochim. Acta* 49 (2004) 313.
- [22] C.-C. Wang, C.-C. Hu, *Mater. Chem. Phys.* 83 (2004) 289.
- [23] Y. Nakamura, S.-I. Suye, J.-I. Kira, H. Tera, I. Tabata, M. Senda, *Biochem. Biophys. Acta* 1289 (1996) 221.
- [24] M. Studnickova, H. Paulova-Klakanova, J. Turanek, J. Kovar, *J. Electroanal. Chem.* 252 (1988) 383.
- [25] Southampton Electrochemistry Group, *Instrumental Methods in Electrochemistry*, Wiley, New York, 1985.
- [26] J. Wang, *Analytical Electrochemistry*, 2nd ed., Wiley/VCH, 2000.
- [27] W.-S. Kim, W.-J. Sim, K.-I. Chung, Y.-E. Sung, Y.-K. Choi, *J. Power Sources* 112 (2002) 76.
- [28] M. Aizawa, R.W. Coughlin, M. Charles, *Biochim. Biophys. Acta* 385 (1975) 362.
- [29] B.A. Boukamp, *Equivalent Circuit Users Manuel Report CT88/265/128*, Department of Chemical Technology, University of Twente, The Netherlands, 1989.
- [30] S. Omanovic, S.G. Roscoe, *Langmuir* 15 (1999) 8315.
- [31] S. Omanovic, S.G. Roscoe, *J. Colloid Interf. Sci.* 227 (2000) 452.
- [32] T. Okamura, *Denki Kagaku* 41 (1973) 303.
- [33] D.E. Brown, D.S. Sholl, R.T. Skodje, S.M. George, *Chem. Phys.* 205 (1996) 23.
- [34] M. Kramer, M. Tomkiewicz, *J. Electrochem. Soc.* 131 (1984) 1283.
- [35] M. Tomkiewicz, B. Aurian-Blajeni, *J. Electrochem. Soc.* 135 (1988) 2743.
- [36] H.S. Lin, *Phys. Rev. Lett.* 55 (1985) 529.
- [37] S. Omanovic, M. Metikos-Hukovic, *Thin Solid Films* 266 (1995) 35.
- [38] H.S. Fogler, *Elements of Chemical Reaction Engineering*, 3rd ed., Prentice-Hall, 1999.
- [39] A.J. Bard, L.R. Faulkner, *Electrochemical Methods: Fundamentals and Applications*, 2nd ed., Wiley, 2001.
- [40] S.E. Yun, M. Taya, S. Tone, *Biotechnol. Lett.* 16 (1994) 1053.
- [41] H. Jaegfeldt, *J. Electroanal. Chem.* 110 (1980) 295.
- [42] I.N. Levine, *Physical Chemistry*, 5th ed., McGraw-Hill, 2002.
- [43] O. Levenspiel, *Chemical Reaction Engineering*, 3rd ed., Wiley, 1999.
- [44] Y. Kashiwagi, Y. Yanagisawa, N. Shibayama, K. Nakahara, F. Kurashima, J.-I. Anzai, T. Osa, *Chem. Lett.* (1996) 1093.